Structure–function analysis of water-soluble inhibitors of the catalytic domain of exotoxin A from *Pseudomonas aeruginosa*

Susan P. YATES*, Patricia L. TAYLOR*, René JØRGENSEN†, Dana FERRARIS‡, Jie ZHANG‡, Gregers R. ANDERSEN†[1] and A. Rod MERRILL*[1]

*Department of Molecular and Cellular Biology, University of Guelph, Guelph, ON, Canada N1G 2W1, †Macromolecular Crystallography, Department of Molecular Biology, University of Aarhus, Gustav Wieds vej 10C, DK8000 Aarhus, Denmark, and ‡Guilford Pharmaceuticals, Baltimore, MD 21224, U.S.A.

The mono-ADPRT (mono-ADP-ribosyltransferase), *Pseudomonas aeruginosa* ETA (exotoxin A), catalyses the transfer of ADP-ribose from NAD^+ to its protein substrate. A series of water-soluble compounds that structurally mimic the nicotinamide moiety of NAD^+ was investigated for their inhibition of the catalytic domain of ETA. The importance of an amide locked into a hetero-ring structure and a core hetero-ring system that is planar was a trend evident by the IC_{50} values. Also, the weaker inhibitors have core ring structures that are less planar and thus more flexible. One of the most potent inhibitors, PJ34, was further characterized and shown to exhibit competitive inhibition with an inhibition constant K_i of 140 nM. We also report the crystal structure of the catalytic domain of ETA in complex with PJ34, the first example of a mono-ADPRT in complex with an inhibitor. The 2.1 Å (1 Å = 0.1 nm) resolution structure revealed that PJ34 is bound within the nicotinamide-binding pocket and forms stabilizing hydrogen bonds with the main chain of Gly-441 and to the side-chain oxygen of Gln-485, a member of a proposed catalytic loop. Structural comparison of this inhibitor complex with diphtheria toxin (a mono-ADPRT) and with PARPs [poly(ADP-ribose) polymerases] shows similarity of the catalytic residues; however, a loop similar to that found in ETA is present in diphtheria toxin but not in PARP. The present study provides insight into the important features required for inhibitors that mimic NAD^+ and their binding to the mono-ADPRT family of toxins.

Key words: bacterial toxin, competitive inhibitor, exotoxin A, mono-ADP-ribosyltransferase, *Pseudomonas aeruginosa*, X-ray crystallography.

INTRODUCTION

The Gram-negative bacillus, *Pseudomonas aeruginosa*, is widespread in the environment with its prevalence related to its ability to inhabit a diverse range of surroundings and consume a variety of carbon and energy sources. Under the appropriate conditions, *P. aeruginosa* has the ability to behave as an opportunistic pathogen and targets those people with compromised immune systems, which includes those suffering from AIDS, burns, cystic fibrosis or cancer. *P. aeruginosa* possesses several potent virulence factors, which in combination with its multidrug resistance, makes treating a *P. aeruginosa* infection difficult [1,2].

One of the most toxic factors secreted by *P. aeruginosa* is ETA (exotoxin A), which has an LD_{50} (50 % of a lethal dose) of 0.2 μg/animal on intraperitoneal injection into mice [3]. ETA is a 66 kDa protein comprised of three distinct domains: receptor-binding (domain I), translocation (domain II) and catalysis (domain III) [4]. ETA enters eukaryotic cells by receptor-mediated endocytosis [5] with the cytoplasm as its end destination, where it catalyses the ADP-ribosylation of its target protein, eEF2 (eukaryotic elongation factor 2). This modification of ADP-ribose on the diphthamide residue of eEF2 leads to its inability to function in protein synthesis with eventual cell death [6,7].

Interactions with the NAD^+ substrate within the active site of ETA are well defined due to several mutagenesis and structural studies, and the identified catalytic residues include Glu-553, His-440, Tyr-481 and Tyr-470 [4,8–10]. In the X-ray structure of the enzyme domain with a substrate analogue, Glu-553 forms a hydrogen bond with the 2′OH of the thiazole-ribose of β-TAD (β-methylene-thiazole-4-carboxamide adenine dinucleotide), where the thiazole moiety is analogous to the nicotinamide segment of the NAD^+ substrate, and this is believed to maintain NAD^+ in a conformation that allows exposure of the scissile N-glycosidic bond [8]. The negatively charged carboxylate of Glu-553 may stabilize a positively charged reaction intermediate, the ribooxocarbenium ion [11]. van der Waals and aromatic ring-stacking interactions occur with the nicotinamide moiety of NAD^+, which stacks between Tyr-481 and Tyr-470. The imidazole side chain of His-440 binds by a hydrogen bond with the AMP-ribose moiety of NAD^+ and with the main chain carbonyl of Tyr-470 [8,12].

The catalytic domain of ETA is functionally and structurally similar to members of both the mono-ADPRTs (mono-ADP-ribosyltransferases) such as DT (diphtheria toxin), which also catalyses the ADP-ribosylation of eEF2 [13], and with the PARPs [poly(ADP-ribose) polymerases] [14–17]. PARPs are situated in the eukaryotic nucleus and they catalyse the covalent attachment of ADP-ribose units from NAD^+ to itself and to a variety of nuclear DNA-binding proteins in response to DNA strand breakage. Hence PARP serves to maintain genome integrity, however, the rapid activation of PARP depletes the NAD^+ concentration within the cell, which disrupts important energy production processes like glycolysis, electron transport and ATP formation leading to cell suicide [18,19]. Therefore several research groups have focused on the inhibition of PARP. Many of the inhibitors that act against PARP are designed to mimic the nicotinamide moiety of NAD^+ [20]. Structures of inhibitors complexed to the PARP enzyme demonstrate that the predominant interactions involve

Abbreviations used: ADPRT, ADP-ribosyltransferase; 5-AIQ, 5-amino-isoquinoline-HCl; β-TAD, β-methylene-thiazole-4-carboxamide adenine dinucleotide; DT, diphtheria toxin; eEF2, eukaryotic elongation factor 2; ε-NAD^+, 1,N^6-etheno-NAD^+; ETA, exotoxin A; LB, Lineweaver–Burk; NAP, 1,8-naphthalimide; PARP, poly(ADP-ribose) polymerase; PE24H, a 24 kDa C-terminal, containing a His_6 tag, of *P. aeruginosa* exotoxin A.

[1] Correspondence may be addressed to either of the authors (email rmerrill@uoguelph.ca and grand@bioxray.dk).

The coordinates and structure factors will appear in Protein Data Bank under the PDB number 1XK9.

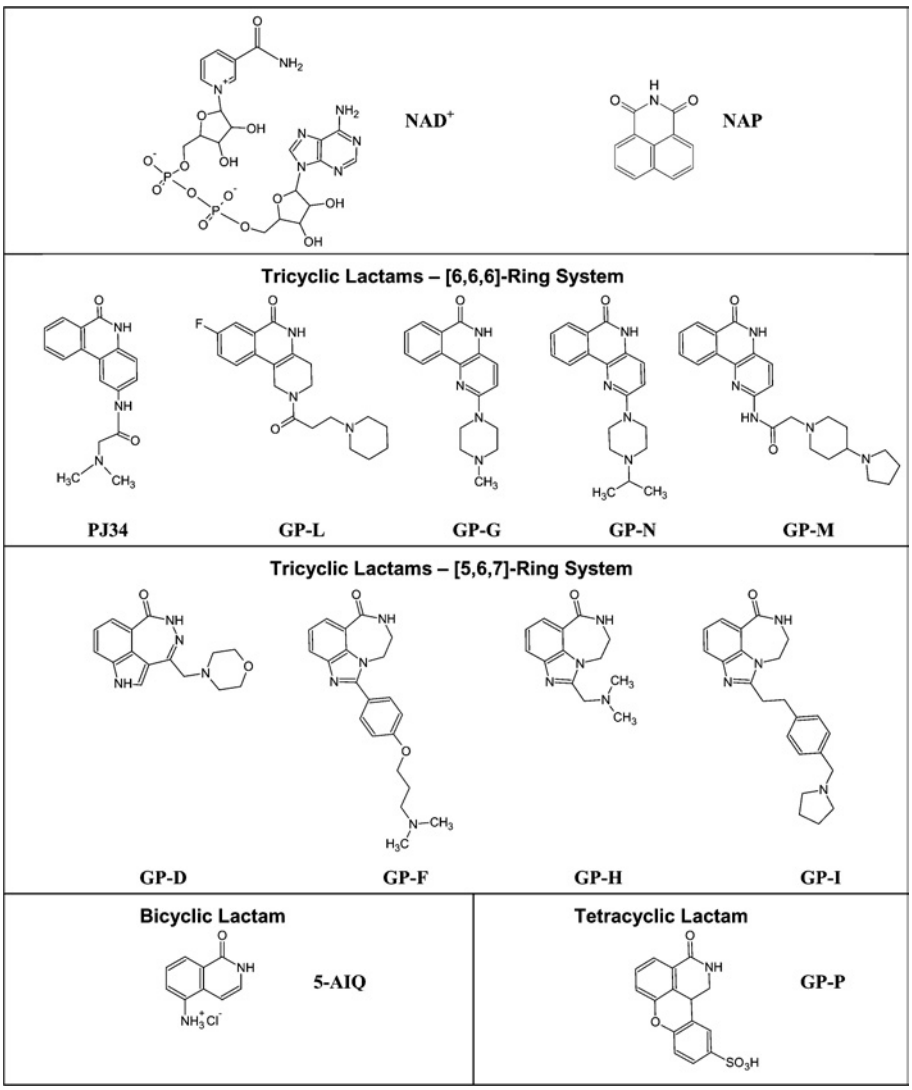

Figure 1 Chemical structures of the ETA inhibitors

The inhibitors are grouped according to their core ring structures. The substrate NAD^+ and the inhibitor NAP are shown for comparison.

the amide or lactam group of the inhibitor hydrogen bonding with the main chain of Gly-863 [14,21,22]. Generally, these PARP inhibitors will also act against the bacterial toxins, like ETA and DT, since a high degree of similarity exists between these proteins, making these inhibitor studies invaluable.

Previously, our research group had characterized a series of small, non-polar competitive inhibitors against ETA. The most potent inhibitor identified in this study was NAP (1,8-naphthalimide) with an IC_{50} value of 87 nM [23]. A model of NAP bound to ETA was proposed that was based on the crystal structures of the catalytic domain of chicken PARP with 4-amino-NAP [21] and the catalytic domain of ETA in complex with β-TAD [8]. In the NAP–ETA model, potential interactions within the nicotinamide-binding pocket were shown, including hydrogen bonds with the main chain Gly-441 equivalent to those observed in PARP [23]. Although this compound and others in this study were effective against the toxin, their lack of water-solubility limits the usefulness of these compounds as potential therapeutic compounds.

In the present study, we describe the *in vitro* characterization of a series of water-soluble inhibitors of the catalytic domain of ETA (PE24H, *P. aeruginosa* exotoxin A 24 kDa C-terminal fragment containing a His_6 tag) through the determination of their IC_{50} values. A more in-depth analysis of the inhibition of PE24H by the compound PJ34 was undertaken, which included characterization of its inhibition kinetics followed by the co-crystal X-ray structure of PE24H with the PJ34 inhibitor. This high-resolution structure reveals important new insights into the interaction of NAD^+ with the mono-ADPRT family of toxins and into some of the chemical features required for tight-binding inhibitors.

EXPERIMENTAL

Potential inhibitors

Compounds tested for inhibition are shown in Figure 1. PJ34 was commercially available from Sigma–Aldrich (St. Louis, MO, U.S.A.), the GP series of compounds was supplied by Guilford Pharmaceuticals (Baltimore, MD, U.S.A.), 5-AIQ (5-amino-isoquinoline-HCl) was commercially available from Alexis Biochemicals (San Diego, CA, U.S.A.). For kinetic analysis, all inhibitor stock solutions were prepared in 50 mM potassium phosphate buffer (pH 7.0), except GP-I, which was dissolved in

MilliQ™ water, and 5-AIQ and PJ34, which were prepared in 20 mM Tris/HCl (pH 7.9). Co-ordinate files for each potential inhibitor were generated using the Dundee PRODRG2 Server [24] and visualized using DS ViewerPro™ version 5.0 (Accelrys, San Diego, CA, U.S.A.).

Overexpression and purification of PE24H

The catalytic fragment of ETA with a C-terminal His_6 tag (PE24H) was overexpressed and purified as described in [25] except that the chelate–agarose affinity column was charged with 100 mM $ZnSO_4$.

Purification of eEF2

eEF2 was purified from either wheat germ [25] or yeast [26] as described previously.

IC_{50} determination for the inhibitory compounds

The substrates, ε-NAD^+ (1,N^6-etheno-NAD^+) and eEF2, in the fluorescence-based ADPRT assay (described previously [25]) were used at saturating doses of 500 and 14 μM respectively, and a range of inhibitor concentrations (dependent on the level of inhibition) were added to the assay medium (20 mM Tris/HCl, pH 7.9) in a 70 μl total volume. The reaction mixture was incubated for 5 min at 25 °C in a disposable UltraVette™ microcuvette (Brand GMBH, Wertheim, Germany). The reaction was initiated by adding 5 nM (final concentration) PE24H. IC_{50}, the concentration of the inhibitor that decreases the activity of the enzyme by 50 %, was determined by non-linear regression curve fitting using Origin 6.1 (OriginLab, Northampton, MA, U.S.A.). The data were fitted to the exponential first-order decay function.

Kinetic analysis of PJ34 inhibition of ADPRT activity

The NAD^+-dependent ADPRT assay was performed as described in [25] with the eEF2 concentration in the assay medium held to 14 μM, whereas the concentrations of ε-NAD^+ were between 0 and 500 μM in the presence of PJ34 at 0, 300, 600 or 1200 nM. The reactions were initiated with 10 nM (final concentration) PE24H. The data were analysed by linear regression analysis of both the Hanes–Woolf and the LB (Lineweaver–Burk) plots. The inhibition constant K_i value was determined using Dixon plots, as well as from secondary plots of the slope of the LB plots versus inhibitor concentration.

Binding affinity of inhibitor compounds to PE24H

The quenching of the intrinsic tryptophan fluorescence of PE24H was used to determine the binding dissociation constant K_D for the inhibitors as described elsewhere [23]. Briefly, the fluorescence quenching of PE24H was measured as a function of the inhibitor concentration. Triplicate reactions were performed over a suitable concentration range of the inhibitor, in the presence of PE24H (1.25 μM final concentration) at 25 °C in an initial volume of 600 μl [50 mM NaCl, 20 mM Tris/HCl (pH 7.9) buffer]. Samples were excited at 295 nm and monitored at an emission of 340 nm. All band passes were set to 4 nm and all measurements were corrected for buffer contribution to the fluorescence signal.

Crystallization of PE24H–PJ34 complex

Purified PE24H protein in 20 mM Tris/HCl, pH 7.6, 100 mM NaCl was concentrated to 11 mg/ml and PJ34 inhibitor, previously dissolved in the same buffer (0.5 mM, final concentration) was added to the protein solution (10 mg/ml, final concentration). The protein–inhibitor mixture was centrifuged at 16 000 ***g*** for 15 min (4 °C) in a microfuge before crystallization. Crystallization trials were conducted at 19 °C using the sitting drop vapour-diffusion method as described previously [12], however, with some modifications. The protein–inhibitor solution (2 μl) was mixed with 2 μl of reservoir solution (500 μl volume) containing various concentrations of sodium citrate buffer (pH 7.5). Optimal crystallization contained 1.1 M sodium citrate buffer, pH 7.5, 0.5 mM dithiothreitol and 0.9 mM NaN_3 in the reservoir solution. Microcrystals were grown for 3–4 days at 19 °C. Larger crystals used for data collection were obtained by streak seeding. These crystals appeared after 3–4 days and reached their final size within 1–2 weeks.

Table 1 Statistics for data collection and refinement

Parameter	Value
Data	
Space group	$P2_12_12_1$
Unit-cell parameters	
a (Å)	56.035
b (Å)	78.680
c (Å)	91.694
Wavelength (Å)	1.046
Resolution (Å)*	35–2.1 (2.3–2.1)
Completeness (%)*	99.8 (100)
Mean $I/\sigma(I)$*	13.35 (7.65)
R_{merge} (%)*†	10.8 (23.6)
Redundancy*	6.8 (6.8)
Refinement	
Reflections	
Used/free	24275/1236
Atoms	
Protein/inhibitor/water	3090/44/391
R-factor (%)*‡	21.33 (24.44)
R_{free}-factor (%)*§	23.46 (26.02)
Resolution for outer shell (Å)	2.13–2.10
R.M.S. deviation	
Bonds (Å)	0.008
Angles (°)	1.449
Ramachandran (%)‖	
Monomer A	98.8/1.2/0
Monomer B	98.7/0.6/0.6¶

* Values in brackets are for outer resolution shell.

† $R_{merge} = (\sum_h \sum_{j=1,N} |I_h - I_h(j)| / \sum_h N \times I_h)$ for the intensity of a reflection measured *N* times.

‡ $R = \sum_h ||F_{obs}| - k|F_{calc}|| / \sum_h |F_{obs}|$, where F_{obs} and F_{calc} are the observed and calculated structure factor respectively and *k* is a scaling factor.

§ R_{free} is identical with *R* on a subset of test reflections not used in refinement.

‖ The statistics for the Ramachandran plot are residues in the most favoured plus additionally favoured regions/generously allowed regions/disallowed regions.

¶ Glu-522 in chain B is involved in crystal contacts with Lys-590 in chain A.

Data collection

Crystals were harvested in stabilization buffer (0.5 mM PJ34 and 1.1 M sodium citrate, pH 7.5) and then rapidly transferred to cryoprotection buffer [0.5 mM PJ34 and 1.1 M sodium citrate, pH 7.5, in 20 % (v/v) glycerol] followed by flash cooling in a N_2 stream at 100 K. Data sets for the toxin–inhibitor crystals were collected at the 911-2 beamline (Maxlab, Lund, Sweden) equipped with a MAR CCD detector (Table 1).

Structure solution and refinement

The crystals of the toxin–PJ34 complex diffracted to 2.1 Å resolution. The data were processed and reduced with XDS [27]. The structure was solved by molecular replacement with MOLREP [28] using 1AER (chain A, residues 399–609) [8] as the model.

Table 2 IC_{50} values for the PE24H inhibitors determined using the fluorescence ADPRT assay

MsOH, mesylate salts.

Code	Compound chemical name	IC_{50} (μM)
GP-D	3-(Morpholin-4-ylmethyl)-1,5-dihydro-6*H*-[1,2]diazepino[4,5,6-cd]indol-6-one	0.17 ± 0.03
PJ34	*N*-(6-oxo-5,6-dihydro-phenanthridin-2-yl)-*N*,*N*-dimethylacetamide	0.28 ± 0.07
GP-M	*N*-(6-oxo-5,6-dihydrobenzo[c][1,5]naphthyridin-2-yl)-2-(4-pyrrolidin-1-ylpiperidin-1-yl)acetamide-HCl	0.29 ± 0.04
GP-P	1,11b-Dihydro-[1]benzopyrano[4,3,2-de]isoquinolin-3(2*H*)-one-10-sulphonic acid	0.45 ± 0.02
GP-F	1-[4-(3-Dimethylamino-propoxy)-phenyl]-8,9-dihydro-7*H*-2,7,9a-triaza-benzo[cd]azulen-6-one-HCl	0.48 ± 0.04
GP-L	8-Fluoro-2-(3-piperidin-1-ylpropanoyl)-1,3,4,5-2*H*-tetrahydrobenzo[c]-1,6-naphthyridin-6-one-MsOH	0.61 ± 0.14
GP-G	2-(4-Methylpiperazin-1-yl)-5*H*-benzo[c][1,5]naphthyridin-6-one-MsOH	0.69 ± 0.13
GP-H	1-Dimethylaminomethyl-8,9-dihydro-7*H*-2,7,9a-triaza-benzo[cd]azulen-6-one-HCl	0.96 ± 0.05
GP-N	2-(4-Isopropylpiperazin-1-yl)-5*H*-benzo[c][1,5]naphthyridin-6-one-MsOH	1.05 ± 0.04
GP-I	1-[2-(4-Pyrrolidin-1-ylmethyl-phenyl)-ethyl]-8,9-dihydro-7*H*-2,7,9a-triaza-benzo[cd]azulen-6-one hydrochloride-HCl	4.46 ± 0.95
5-AIQ	5-Amino-isoquinoline-HCl	22.8 ± 2.7

The model was completed and rebuilt with the refinement program O [29] and refined with CNS (crystallography and NMR system) [30] using first strict NCS (non-crystallographic symmetry) and later NCS restraints on the two toxin–PJ34 complexes in the asymmetric unit. A co-ordinate file as well as CNS parameter and topology files was generated for PJ34 using the Dundee PRODRG2 Server [24]. The quality of both chains of the structure was inspected with PROCHECK [31] after refinement. All figures were created in PyMOL [32].

Structure alignments

The PE24H–PJ34 structure was superimposed on the previous structure of the catalytic domain of ETA in complex with β-TAD (1AER [8]), as well as the catalytic domains from both DT (1TOX [13]) and PARP (1PAX [14], 2PAX, 3PAX and 4PAX [21]) using either the least-squares function in O [29] or Swiss-PDB Viewer, version 3.7 [33].

RESULTS

Inhibitor structures

The structures of the water-soluble inhibitors are shown in Figure 1 and the common structural motif among these compounds is a benzamido group fused into a hetero-ring structure; this functional group mimics the nicotinamide moiety of NAD^+. Previously, studies on PARP inhibition demonstrated that when the amide substituent of the benzamido group is locked in the more favoured s-trans conformation then this facilitates interaction with active site residues leading to an increase in the inhibition potency of a compound [22,34]. Several strong inhibitors against ETA have been studied, e.g. NAP [23]; however, these were not suitable for clinical studies due to their lack of water solubility. Therefore the compounds investigated in the present study contain hetero-rings with R-group substitutions that include the addition of hydrogen donors and/or acceptors to increase their water solubility.

The water-soluble compounds are classified according to their ring systems in Figure 1. The categories include bicyclic, tricyclic and tetracyclic lactams. The tricyclic lactams are further subdivided into [6,6,6]- and [5,6,7]-ring systems. In the [6,6,6]-system class, PJ34 is an 5-[*H*]-phenanthridin-6-one based compound [18,35,36], whereas GP-L [37], GP-G, GP-M and GP-N are aza-5[*H*]-phenanthridin-6-ones [38]. In the [5,6,7]-system class, GP-F, GP-H and GP-I are imidazobenzodiazepines derivatized at the benzimidazoles [34] and GP-D is comprised of both an indole and seven-membered lactam ring. The bicyclic lactam class contains 5-AIQ (an isoquinoline), the tetracyclic class contains GP-P {a tetraheterocyclic lactam derivative of GPI-6150 (1,11b-dihydro-[2*H*]benzopyrano[4,3,2-de]isoquinolin-3-one) a novel inhibitor of PARP [39]}.

Inhibition of ADPRT and IC_{50} values

Each of the water-soluble compounds was initially assessed for their ability to inhibit the ADPRT activity of the toxin. The IC_{50} values were determined from full dose–response curves (results not shown) and these inhibition values ranged from 170 nM for GP-D to 22.8 μM for 5-AIQ (Table 2). To correlate the level of inhibition to the structure of the compound, the co-ordinate files for each inhibitor molecule were created using PRODRG2 [24]. Some of the notable features important for inhibition were observed (see the Discussion section).

Inhibition kinetics of PJ34

PJ34 has previously been characterized both in *in vitro* and *in vivo* studies of PARP enzymes. It is one of the most potent inhibitors against the catalytic domain of ETA, having an IC_{50} value of 280 nM (Table 2). Therefore a more detailed analysis of its inhibition was undertaken. For the NAD^+-dependent ADPRT activity, the Michaelis constant K_M and maximal velocity V_{max} values for PE24H were determined in the presence of the inhibitor PJ34. The inhibition of the toxin by PJ34 is competitive since the V_{max} value is unaffected, whereas the K_M value increases with increasing PJ34 concentration. The K_M values increased from 121 μM (no PJ34) to 582 μM (1200 nM PJ34). Figure 2(A) shows the Dixon plot for the inhibition of PE24H by PJ34. Using the re-plot of the slopes from the Dixon plot (Figure 2B), the K_i for these data was determined to be 140 nM, which agrees with the K_i value calculated using the LB method (results not shown).

On binding to the enzyme, PJ34 quenched the intrinsic tryptophan fluorescence of PE24H. Figure 2(C) shows the fluorescence quench curve for the intrinsic tryptophan fluorescence of PE24H on titration with PJ34 as the ligand. The K_D value for PJ34 binding to PE24H is 820 ($\pm$ 54) nM and this represents approx. 70 times tighter binding to the enzyme when compared with NAD^+.

Structure description of toxin–PJ34 complex

The crystal structure of the catalytic domain of ETA in complex with the inhibitor PJ34 was determined at 2.1 Å resolution. The two toxin molecules in the asymmetric unit are in a very similar conformation with only minor differences. The overall structure of the toxin–PJ34 complex is highly comparable with previously determined structures for the catalytic domain of ETA in complex with either β-TAD [8] or hydrolysed NAD^+ [12]. The structure

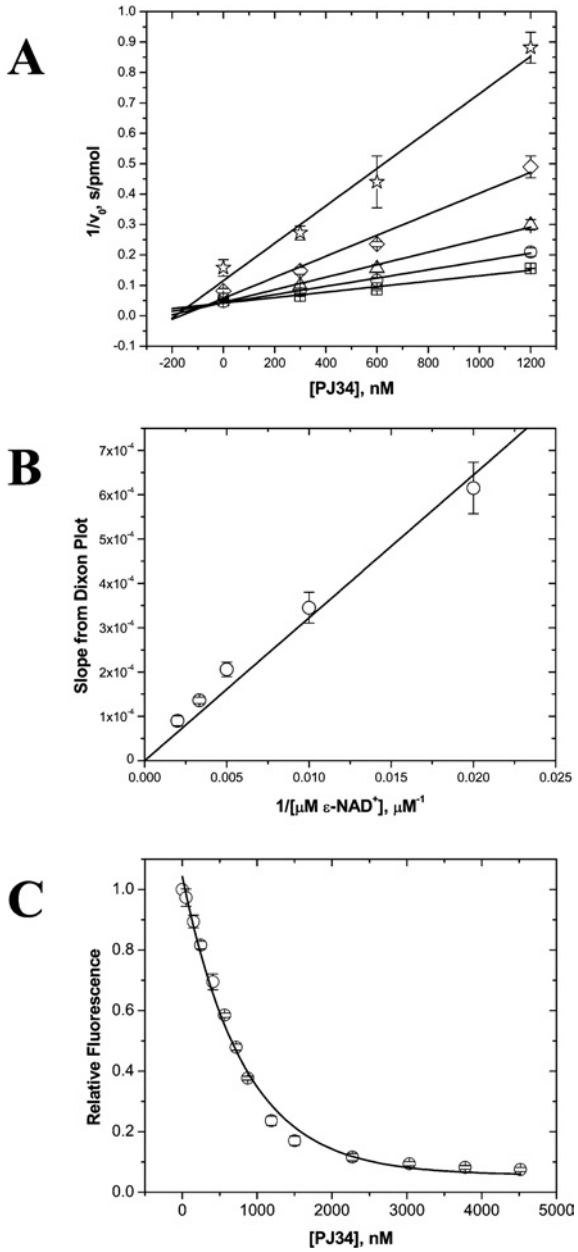

Figure 2 Inhibitory properties of PJ34 against PE24H

(**A**) The Dixon plot for PJ34 in the presence of different fixed concentrations of substrate, ε-NAD^+. The ADPRT activity of PE24H at 50 (☆), 100 (◇), 200 (△), 300 (○) and 500 (□) μM ε-NAD^+. v_0, initial velocity. (**B**) The re-plot of the slopes of the Dixon plot where the slope is equal to $K_M/(V_{max}K_i)$. The K_M and V_{max} values for the NAD^+-dependent ADPRT reaction are 121 μM and 26.7 pmol/s respectively. The assay included 20 mM Tris/HCl, pH 7.9, 0–500 μM ε-NAD^+, 14 μM eEF2, 0–1200 nM PJ34 and 10 nM PE24H in a total volume of 70 μl. (**C**) Binding of PJ34 to PE24H by quenching of intrinsic protein fluorescence. The titration was conducted in 20 mM Tris/HCl, pH 7.9, 50 mM NaCl at 25 °C using 1.25 μM toxin. The fluorescence excitation was at 295 nm with fluorescence emission at 340 nm (at band passes set to 4 nm). The data were corrected for the dilution effect.

consists of residues 399–602 (amino acid numbering based on the sequence of the whole, mature toxin) with the exception of the loop encompassing residues 459–464, which could not be modelled in monomer B. This loop region in monomer B had weak electron density probably due to local disorder as previously observed in other structures of the catalytic domain of ETA [8,12]. Notably, in monomer A, the electron density for this loop could be traced. It appears to be involved in interactions with the N-terminus of a symmetry-related molecule of monomer B. Both the N-terminus of this symmetry-related molecule and the loop, although resolved, have high mobility as dictated by the weaker electron density compared with the remainder of the protein structure. The loop adopts an altered conformation when compared with earlier structures and may represent an orientation that is a stable alternative (Figure 3A). However, the C-terminus of both monomers could only be resolved as far as residue 602, again due to the absence of electron density in this presumably flexible terminus of the protein. The Ramachandran plots for monomer A show residues Gln-460 and Asp-463 in the generously allowed region. Both these residues are located in the loop consisting of residues 459–464 mentioned above. In monomer B, Glu-522 is found on the edge of the disallowed region in the Ramachandran plot. Importantly, a well-defined electron density is present for this residue, but a crystal packing artifact probably causes the unusual main chain conformation induced by a salt bridge with Lys-590 of monomer A.

Since monomer A was more complete than monomer B, all further analysis was based on the former molecule. The PJ34 inhibitor is situated in a hydrophobic pocket of the toxin with approx. 60 % of its surface buried by interaction with the toxin (determined using CNS [30]). This represents the same pocket in which nicotinamide binds in the structures of the catalytic domain of both ETA and DT. The pocket is formed by residues His-440, Gly-441, Tyr-470, Ile-471, Ala-472, Leu-477, Ala-478 and Tyr-481 (Figure 3B, pocket shown in yellow).

The electron density of the hetero-ring system of the inhibitor is clearly defined, allowing reliable positioning of the rings into the active site of the toxin (Figure 3C). However, the electron density is weaker for the terminus of the R-group (tertiary amine) of PJ34 suggesting some flexibility in the 'arm' of the inhibitor. Despite this, the electron density for the R-group favours its direction towards the loop containing Gln-485.

The bound PJ34 inhibitor is stabilized within the active site of the toxin through hydrophobic interactions and hydrogen bonds (Figure 3D). The first hydrogen bond is between the main chain nitrogen of Gly-441 and the carbonyl of PJ34 (2.5 Å) and the second is between the main chain oxygen of Gly-441 and the amide nitrogen of PJ34 (2.5 Å). The last potential hydrogen bond exists between the tertiary amine on the R-group of PJ34 and the side-chain oxygen of Gln-485 situated 3.1 Å away. The phenyl moiety of Tyr-481 forms van der Waals interactions with PJ34, positioned approx. 4 Å away. The planes of the two aromatic rings are almost parallel favouring π–π interactions. Tyr-470 is also adjacent to the hetero-ring system, however, it is 6–7 Å from PJ34 and at an angle of 40° and, therefore, it is unable to form strong stacking interactions similar to those of Tyr-481. However, when β-TAD is bound within the active site Tyr-470 lies more in plane with the thiazole moiety (Figure 4A). An additional hydrogen bond also occurs between ND1-His-440 and the main chain oxygen of Tyr-470 (2.7 Å) thus stabilizing these important catalytic residues within the active site.

DISCUSSION

When the level of inhibition (Table 2) of the water-soluble inhibitory compounds is correlated to their structures (Figure 1) some trends are evident. The bicyclic lactam, 5-AIQ, although it does fix the amide in the s-trans conformation, does not compete as strongly as many of the other test compounds against NAD^+ for the nicotinamide-binding pocket within the enzyme. In general, the more potent inhibitors have a core ring structure that is planar (PJ34, GP-D and GP-M). The exceptions are GP-G and

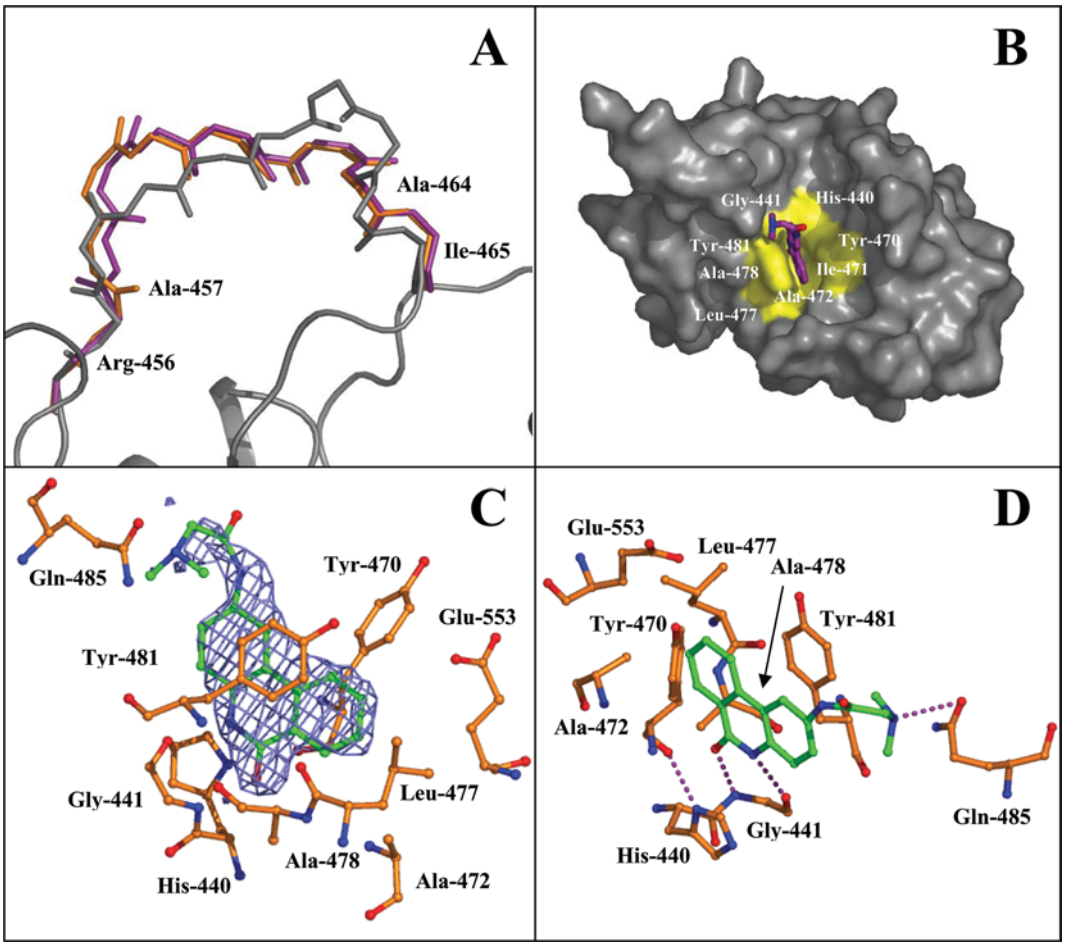

Figure 3 Structure of PE24H–PJ34

(**A**) Superposition of the modelled loop from the catalytic domain of ETA (PE24H) in complex with PJ34 [monomer A (shown in grey)] compared with the loops from previous ETA structures. The loop from the catalytic domain of ETA in complex with either β-TAD (shown in purple, monomer B; PDB number 1AER [8]) or hydrolysed NAD^+ (shown in orange, monomer B; PDB number 1DMA [12] are illustrated. The main chain is shown from residues 456 to 465. (**B**) The PJ34 inhibitor bound within the active site of the toxin. The hydrophobic pocket is shown in yellow and the inhibitor in purple. This hydrophobic pocket comprises the residues His-440, Gly-441, Tyr-470, Ile-471, Ala-472, Leu-477, Ala-478 and Tyr-481. (**C**) The $2F_{obs}$-F_{calc} omit map of PJ34 bound to monomer A within the active site of ETA contoured at 1σ. Phases for the map were calculated with no contribution from the PJ34 atoms. (**D**) The binding of the inhibitor PJ34 to PE24H. PJ34 is shown in green and important toxin residues involved in hydrogen bonding (broken lines) or hydrophobic interactions are shown.

GP-N, which have the same planar hetero-ring core as GP-M, one of the stronger inhibitors, but have higher IC_{50} values (Table 2). The differences seem to originate in the R-group substitution at the 2-position (Figure 1). GP-G and GP-N both contain piperazine moieties as their R-groups, whereas GP-M contains an amide derivative more like PJ34 than the piperazine derivatives. Therefore planarity of the core ring structure is important but the R-group substitutions also affect the level of inhibition. The best inhibitor, GP-D, contains a unique seven-membered ring and an indole. In PARP enzymes, indole tricyclic compounds were ideal since the indole group could hydrogen bond with Glu-988 (analogous to Glu-553 in ETA) through a water molecule [22]. This additional hydrogen bond may serve as the basis to rationalize the greater inhibition seen for GP-D. The weaker inhibitors have core ring structures that are less planar and thus more flexible. Apparently, the active site of the toxin prefers compounds that have a more rigid and compact conformation which are not ring puckered within the nicotinamide-binding pocket. For GP-F, GP-H and GP-I, some of the ring distortion occurs in the seven-membered ring, which holds the important amide. This slight alteration in planarity may affect the positioning of the predicted hydrogen bonds that mate with Gly-441 within the active site. GP-P also lacks planarity for the amide functionality. However, GP-L does maintain the benzamido group in the same plane, yet the third ring is not planar and thus illustrates the importance of a planar, compact structure for active site binding.

The PJ34 inhibitor is a water-soluble phenanthridinone derivative originally synthesized to target PARP [18]. PJ34 is a well-characterized compound with several *in vitro* and *in vivo* studies performed to date on the protective attributes of this inhibitor in PARP-related systems. Some examples of *in vitro* systems involving PJ34 include the ability of the phenanthridinone to suppress the production of pro-inflammatory cytokines and chemokines in immunostimulated macrophages and to provide protection for murine thymocytes exposed to cytotoxic oxidants [36]. The protective benefits of PJ34 *in vivo* systems involving PARP hyperstimulation include stroke [18], ischaemia caused by heart transplantation [40], diabetic endothelial dysfunction [35] and heart-related conditions induced by side effects caused by cytotoxic drugs [41].

PJ34 is also a potent inhibitor of the catalytic domain of ETA with a low IC_{50} value of 280 nM (Table 2). Subsequently, the

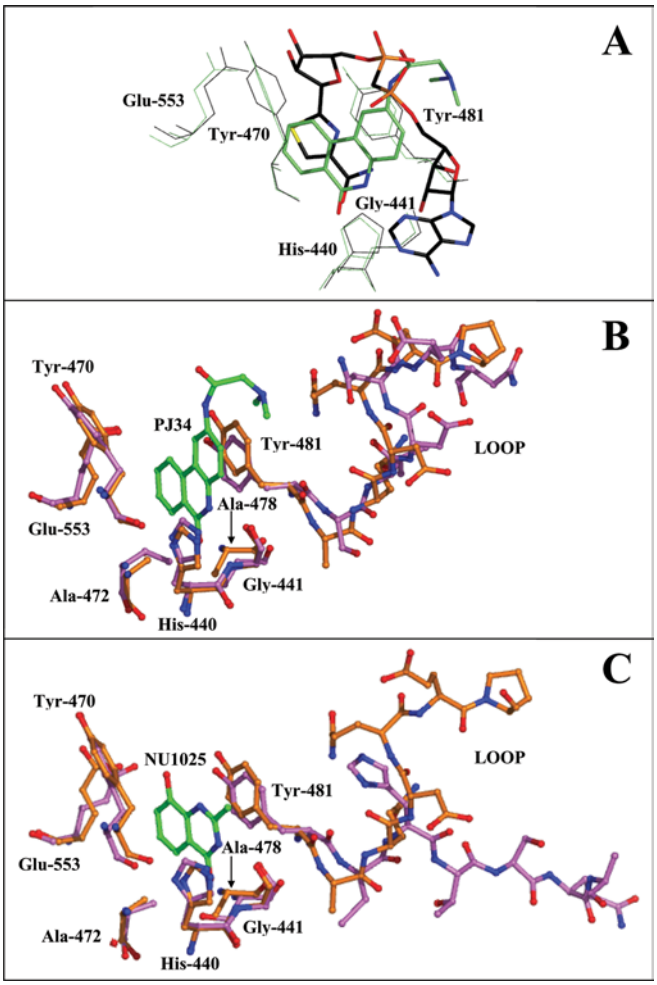

Figure 4 Comparison of PE24H–PJ34 with the active sites from ETA (with β-TAD bound), DT and PARP

(**A**) Superposition of the structure of PE24H–PJ34 (shown in lime green) on the catalytic domain of ETA in complex with β-TAD, an NAD^+-analogue (shown in black; PDB number 1AER [8]). β-TAD contains a thiazole substituent that mimics nicotinamide. (**B**, **C**) Superposition of the structure of PJ34–PE24H (shown in orange) with (**B**) DT (shown in pink; PDB number 1TOX [13]) or (**C**) PARP-NU1025 (shown in pink; PDB number 4PAX [21]). The segment that includes a portion of the catalytic loop of ETA (termed LOOP) is shown and encompasses residues 482–487 in ETA, 66–71 in DT or 908–913 in PARP. In the DT comparison (**B**), the PJ34 inhibitor (green) is shown, whereas in the PARP comparison (**C**) the PARP inhibitor NU1025, 8-hydroxy-2-methyl-3-hydro-quinazolin-4-one (green), is shown and the PJ34 ligand omitted, to demonstrate the same relative orientation of a PARP inhibitor within the toxin active site as PJ34.

mechanism of inhibition by PJ34 was further characterized and shown to follow the competitive model of inhibition possessing a K_i value of 140 nM (Figures 2A and 2B). It is not surprising that PJ34 is a competitive inhibitor since its structure was designed to mimic the nicotinamide moiety of NAD^+ and, therefore, would be expected to compete for the nicotinamide-binding pocket within ETA. The K_D [820 nM (Figure 2C)] and the K_i values are not equal despite both constants representing essentially the same equilibrium. However, the binding affinity of PJ34 to the toxin (K_D) was measured in the absence of the eEF2 substrate, hence, the possibility exists that when eEF2 binds to the toxin a conformation is induced that increases the binding affinity of PJ34 for the toxin as represented by the lower K_i compared with the K_D value.

This is the first report of an X-ray crystal structure of an inhibitor with a mono-ADPRT enzyme. The inhibitor (PJ34) was clearly bound within the active site of ETA and the structure was solved to 2.1 Å resolution. Previously, structures of the PARP enzyme co-crystallized with inhibitors [14,21,22] served as models to deduce how an inhibitor may interact within the active site of the diphthamide-specific mono-ADPRTs, including ETA and DT. The catalytic domain of ETA shows significant common functional and structural properties with DT (the only other known member of the diphthamide-specific mono-ADPRT enzyme subclass) and with the PARPs. The PE24H–PJ34 structure herein confirms that the amide of the benzamino group, designed to mimic nicotinamide, hydrogen bonds with the main chain of Gly-441 (Figure 3D) as was seen when the NAD^+ analogue, β-TAD, was co-crystallized with ETA [8]. These hydrogen bonds are analogous to Gly-22 in DT and Gly-863 in PARP. In the PARP family, an additional hydrogen bond exists between Ser-904 and the lactam carbonyl moiety; however, in both ETA and DT this position is substituted with an alanine residue. This offers a point of discrimination between the poly-ADPRTs and the diphthamide-specific mono-ADPRTs. In addition, PARP was previously crystallized with two tricyclic compounds that both contained a non-planar seven-membered lactam ring; it was postulated that this more flexible conformation allowed the ligand to position closer to those residues involved in these critical hydrogen bonds [22]. However, our inhibition data in the present study suggest that lack of planarity for the core hetero-ring system decreases the inhibition potency of a compound. The hydrophobic nicotinamide-binding pocket for ETA (Figure 3B) may be more selective regarding the size and shape of compounds that it can accommodate compared with the PARP enzymes. PJ34, a planar compound, is sandwiched between the parallel walls of the non-polar, nicotinamide-binding pocket (Figure 3B). Although the important catalytic residues are conserved between ETA and PARP, the walls of this pocket may possess subtle differences probably due to the non-conserved residues, resulting in nicotinamide-binding pockets with selective preferences that act as filters for inhibitor compounds. Therefore, the PARP active site cleft may be more accommodating than ETA to non-planar, more flexible ligands, whereas the nicotinamide-binding pocket of ETA is more stringent and requires ligands with structures that possess a higher degree of planar character.

The X-ray structure of PE24H in complex with PJ34 is highly homologous with the previous structure in complex with the NAD^+ analogue, β-TAD, with only slightly observable differences between their backbone structures. The catalytic residues within the nicotinamide-binding pocket are similarly positioned in both structures (Figure 4A). The exception is Tyr-470, which is rotated away from the planar ring system of PJ34 reducing the π–π stacking interactions seen when β-TAD is bound. The locked amide of the hetero-ring system of PJ34 and the amide substituent on the thiazole group of β-TAD are positioned similarly within the active site, thus allowing the hydrogen bonds with the main chain of Gly-441 to mate.

The structure of PE24H–PJ34 was superimposed with the catalytic domains from DT and PARP (Figures 4B and 4C). As expected, the protein structure housing the important catalytic residues within these proteins is structurally homologous. The catalytic residues of ETA overlay with those in DT and PARP; these include, His-440 (His-21, DT; His-862, PARP), Gly-441 (Gly-22, DT; Gly-863, PARP), Tyr-470 (Tyr-54, DT; Tyr-896, PARP), Tyr-481 (Tyr-65, DT; Tyr-907, PARP) and Glu-553 (Glu-148, DT; Glu-988, PARP) (Figures 4B and 4C).

In the PE24H–PJ34 structure, a potential hydrogen bond originates from the tertiary amine of the ligand to the side chain oxygen of Gln-485 (Figure 3D). Gln-485 is a member of an active-site loop that was previously proposed, based on substrate binding

and kinetic data, to modulate the transferase activity of the toxin. Through sequence alignment and molecular modelling a similar loop was identified in DT; thus, this region may represent a diphthamide-specific ADPRT structural motif [42]. When the structures of the catalytic domain of DT and PE24H–PJ34 are superimposed, it is evident that these loops are in a highly similar orientation (Figure 4B). An asparagine residue (position 69) in DT is a conservative substitution for Gln-485 in ETA. Although Asn-69 of DT has a shorter side chain than the corresponding residue in ETA, the flexibility of loop regions may still allow a hydrogen bond with the tertiary amine of PJ34 to occur. However, even in ETA, this hydrogen bond is rather weak (3.1 Å in length). Therefore if derivatives based on PJ34 are created in which the R-group is extended to allow for closer interactions with Gln-485 (or alternatively Asn-69 in DT) then more potent inhibitory compounds may be developed.

The PARP structure chosen for comparison with PE24H–PJ34 is that of the catalytic domain of PARP in complex with the inhibitor NU1025 [21]. Although the active sites of all available PARP–inhibitor complexes superimposed similarly on PE24H–PJ34, the PARP structure with NU1025 bound was chosen since this ligand represents the one most structurally similar to PJ34, including its planarity. In Figure 4(C), the PJ34 ligand in PE24H has been omitted to demonstrate that the inhibitor NU1025 is similarly bound within the PARP enzyme, further substantiating the active site structural homology that exists between the diphthamide-specific ADPRTs and PARP (the spatial positioning of PJ34 is represented in Figure 4B). However, a notable difference between these superimposed structures occurs in the area of the catalytic loop of ETA. The corresponding region in PARP is not structurally similar and may account for differences in its target substrate compared with DT and ETA. Since this difference between DT/ETA and PARP exists, new inhibitors could be designed whereby interactions with this particular region would be targeted to inhibit either DT or ETA without adversely affecting PARP. In contrast, since it is conceivable that the bacterial enzymes (DT and ETA) mimic the endogenous eukaryotic ribosyltransferases that serve to regulate the function of eEF2 at the ribosome [16,17], then the development of inhibitors that are selective for only the PARP enzymes is also an important consideration.

We thank G. Prentice for purification of both wheat and yeast eEF2 and the staff at Cassiopaia, MAXlab, for assistance during data collection. We also thank Dr W. Tam for a careful reading of the manuscript. This study was supported by the Canadian Cystic Fibrosis Foundation (CCFF) and the Canadian Institutes of Health Research (CIHR) grants to A.R.M., the Benzon Foundation and Dansync grant to G.R.A., CCFF Doctoral Studentship to S.P.Y. and CCFF Summer Studentship to P.L.T.

REFERENCES

1 Van Delden, C. and Iglewski, B. H. (1998) Cell-to-cell signaling and Pseudomonas aeruginosa infections. Emerg. Infect. Dis. **4**, 551–560

2 Lyczak, J. B., Cannon, C. L. and Pier, G. B. (2000) Establishment of Pseudomonas aeruginosa infection: lessons from a versatile opportunist. Microbes Infect. **2**, 1051–1060

3 Iglewski, B. H. and Sadoff, J. C. (1979) Toxin inhibitors of protein synthesis: production, purification, and assay of Pseudomonas aeruginosa toxin A. Methods Enzymol. **60**, 780–793

4 Allured, V. S., Collier, R. J., Carroll, S. F. and McKay, D. B. (1986) Structure of exotoxin A of Pseudomonas aeruginosa at 3.0-Angstrom resolution. Proc. Natl. Acad. Sci. U.S.A. **83**, 1320–1324

5 FitzGerald, D., Morris, R. E. and Saelinger, C. B. (1980) Receptor-mediated internalization of Pseudomonas toxin by mouse fibroblasts. Cell (Cambridge, Mass.) **21**, 867–873

6 Foley, B. T., Moehring, J. M. and Moehring, T. J. (1995) Mutations in the elongation factor 2 gene which confer resistance to diphtheria toxin and Pseudomonas exotoxin A. Genetic and biochemical analyses. J. Biol. Chem. **270**, 23218–23225

7 Nygard, O. and Nilsson, L. (1990) Translational dynamics. Interactions between the translational factors, tRNA and ribosomes during eukaryotic protein synthesis. Eur. J. Biochem. **191**, 1–17

8 Li, M., Dyda, F., Benhar, I., Pastan, I. and Davies, D. R. (1996) Crystal structure of the catalytic domain of Pseudomonas exotoxin A complexed with a nicotinamide adenine dinucleotide analog: implications for the activation process and for ADP ribosylation. Proc. Natl. Acad. Sci. U.S.A. **93**, 6902–6906

9 Lukac, M. and Collier, R. J. (1988) Pseudomonas aeruginosa exotoxin A: effects of mutating tyrosine-470 and tyrosine-481 to phenylalanine. Biochemistry **27**, 7629–7632

10 Han, X. Y. and Galloway, D. R. (1995) Active site mutations of Pseudomonas aeruginosa exotoxin A. Analysis of the His440 residue. J. Biol. Chem. **270**, 679–684

11 Parikh, S. L. and Schramm, V. L. (2004) Transition state structure for ADP-ribosylation of eukaryotic elongation factor 2 catalyzed by diphtheria toxin. Biochemistry **43**, 1204–1212

12 Li, M., Dyda, F., Benhar, I., Pastan, I. and Davies, D. R. (1995) The crystal structure of Pseudomonas aeruginosa exotoxin domain III with nicotinamide and AMP: conformational differences with the intact exotoxin. Proc. Natl. Acad. Sci. U.S.A. **92**, 9308–9312

13 Bell, C. E. and Eisenberg, D. (1996) Crystal structure of diphtheria toxin bound to nicotinamide adenine dinucleotide. Biochemistry **35**, 1137–1149

14 Ruf, A., Mennissier de Murcia, J., de Murcia, G. and Schulz, G. E. (1996) Structure of the catalytic fragment of poly(ADP-ribose) polymerase from chicken. Proc. Natl. Acad. Sci. U.S.A. **93**, 7481–7485

15 Bell, C. E., Yeates, T. O. and Eisenberg, D. (1997) Unusual conformation of nicotinamide adenine dinucleotide (NAD) bound to diphtheria toxin: a comparison with NAD bound to the oxidoreductase enzymes. Protein Sci. **6**, 2084–2096

16 Han, S. and Tainer, J. A. (2002) The ARTT motif and a unified structural understanding of substrate recognition in ADP-ribosylating bacterial toxins and eukaryotic ADP-ribosyltransferases. Int. J. Med. Microbiol. **291**, 523–529

17 Koch-Nolte, F. and Haag, F. (1997) Mono (ADP-ribosyl) transferases and related enzymes in animal tissue: emerging gene families. In ADP-ribosylation in Animal Tissue (Haag, F. and Koch-Nolte, F., eds.), pp. 1–13, Plenum Press, New York

18 Abdelkarim, G. E., Gertz, K., Harms, C., Katchanov, J., Dirnagl, U., Szabo, C. and Endres, M. (2001) Protective effects of PJ34, a novel, potent inhibitor of poly(ADP-ribose) polymerase (PARP) in *in vitro* and *in vivo* models of stroke. Int. J. Mol. Med. **7**, 255–260

19 Chiarugi, A. (2002) Poly(ADP-ribose) polymerase: killer or conspirator? The 'suicide hypothesis' revisited. Trends Pharmacol. Sci. **23**, 122–129

20 Li, J. H., Serdyuk, L., Ferraris, D. V., Xiao, G., Tays, K. L., Kletzly, P. W., Li, W., Lautar, S., Zhang, J. and Kalish, V. J. (2001) Synthesis of substituted 5[H]phenanthridin-6-ones as potent poly(ADP-ribose)polymerase-1 (PARP1) inhibitors. Bioorg. Med. Chem. Lett. **11**, 1687–1690

21 Ruf, A., de Murcia, G. and Schulz, G. E. (1998) Inhibitor and NAD^+ binding to poly(ADP-ribose) polymerase as derived from crystal structures and homology modeling. Biochemistry **37**, 3893–3900

22 Canan Koch, S. S., Thoresen, L. H., Tikhe, J. G., Maegley, K. A., Almassy, R. J., Li, J., Yu, X. H., Zook, S. E., Kumpf, R. A., Zhang, C. et al. (2002) Novel tricyclic poly(ADP-ribose) polymerase-1 inhibitors with potent anticancer chemopotentiating activity: design, synthesis, and X-ray cocrystal structure. J. Med. Chem. **45**, 4961–4974

23 Armstrong, S., Li, J. H., Zhang, J. and Merrill, A. R. (2002) Characterization of competitive inhibitors for the transferase activity of Pseudomonas aeruginosa exotoxin A. J. Enzyme Inhib. Med. Chem. **17**, 235–246

24 van Aalten, D. M., Bywater, R., Findlay, J. B., Hendlich, M., Hooft, R. W. and Vriend, G. (1996) PRODRG, a program for generating molecular topologies and unique molecular descriptors from coordinates of small molecules. J. Comput. Aided Mol. Des. **10**, 255–262

25 Armstrong, S. and Merrill, A. R. (2001) Application of a fluorometric assay for characterization of the catalytic competency of a domain III fragment of Pseudomonas aeruginosa exotoxin A. Anal. Biochem. **292**, 26–33

26 Jorgensen, R., Carr-Schmid, A., Ortiz, P. A., Kinzy, T. G. and Andersen, G. R. (2002) Purification and crystallization of the yeast elongation factor eEF2. Acta Crystallogr. D Biol. Crystallogr. **58**, 712–715

27 Kabsch, W. (1993) Automatic processing of rotation diffraction data from crystals of initially unknown symmetry and cell constants. J. Appl. Cryst. **26**, 795–800

28 Vagin, A. and Teplyakov, A. (1997) MOLREP: an automated program for molecular replacement. J. Appl. Cryst. **30**, 1022–1025

29 Jones, T. A., Zou, J. Y., Cowan, S. W. and Kjeldgaard, M. (1991) Improved methods for building protein models in electron density maps and the location of errors in these models. Acta Crystallogr. A **47**, 110–119

30 Brunger, A. T., Adams, P. D., Clore, G. M., DeLano, W. L., Gros, P., Grosse-Kunstleve, R. W., Jiang, J. S., Kuszewski, J., Nilges, M., Pannu, N. S. et al. (1998) Crystallography & NMR system: a new software suite for macromolecular structure determination. Acta Crystallogr. D Biol. Crystallogr. **54**, 905–921

31 Laskowski, R. A., MacArthur, M. W., Moss, D. S. and Thornton, J. M. (1993) PROCHECK: a program to check the stereochemical quality of protein structures. J. Appl. Cryst. **26**, 283–291
32 DeLano, W. L. (2002) The PyMOL User's Manual, DeLano Scientific, San Carlos, CA, U.S.A.
33 Guex, N. and Peitsch, M. C. (1997) SWISS-MODEL and the Swiss-PdbViewer: an environment for comparative protein modeling. Electrophoresis **18**, 2714–2723
34 Ferraris, D., Ficco, R. P., Dain, D., Ginski, M., Lautar, S., Lee-Wisdom, K., Liang, S., Lin, Q., Lu, M. X., Morgan, L. et al. (2003) Design and synthesis of poly(ADP-ribose) polymerase-1 (PARP-1) inhibitors. Part 4: biological evaluation of imidazobenzodiazepines as potent PARP-1 inhibitors for treatment of ischemic injuries. Bioorg. Med. Chem. **11**, 3695–3707
35 Garcia, S. F., Virag, L., Jagtap, P., Szabo, E., Mabley, J. G., Liaudet, L., Marton, A., Hoyt, D. G., Murthy, K. G., Salzman, A. L. et al. (2001) Diabetic endothelial dysfunction: the role of poly(ADP-ribose) polymerase activation. Nat. Med. **7**, 108–113
36 Jagtap, P., Soriano, F. G., Virag, L., Liaudet, L., Mabley, J., Szabo, E., Hasko, G., Marton, A., Lorigados, C. B., Gallyas, Jr, F. et al. (2002) Novel phenanthridinone inhibitors of poly(adenosine 5′-diphosphate-ribose) synthetase: potent cytoprotective and antishock agents. Crit. Care Med. **30**, 1071–1082

Received 31 August 2004/24 September 2004; accepted 30 September 2004
Published as BJ Immediate Publication 30 September 2004, DOI 10.1042/BJ20041480

37 Ferraris, D., Ficco, R. P., Pahutski, T., Lautar, S., Huang, S., Zhang, J. and Kalish, V. (2003) Design and synthesis of poly(ADP-ribose)polymerase-1 (PARP-1) inhibitors. Part 3: *in vitro* evaluation of 1,3,4,5-tetrahydro-benzo[c][1,6]- and [c][1,7]-naphthyridin-6-ones. Bioorg. Med. Chem. Lett. **13**, 2513–2518
38 Ferraris, D., Ko, Y. S., Pahutski, T., Ficco, R. P., Serdyuk, L., Alemu, C., Bradford, C., Chiou, T., Hoover, R., Huang, S. et al. (2003) Design and synthesis of poly ADP-ribose polymerase-1 inhibitors. 2. Biological evaluation of aza-5[H]-phenanthridin-6-ones as potent, aqueous-soluble compounds for the treatment of ischemic injuries. J. Med. Chem. **46**, 3138–3151
39 Zhang, J., Lautar, S., Huang, S., Ramsey, C., Cheung, A. and Li, J. H. (2000) GPI 6150 prevents H_2O_2 cytotoxicity by inhibiting poly(ADP-ribose) polymerase. Biochem. Biophys. Res. Commun. **278**, 590–598
40 Szabo, G., Bahrle, S., Stumpf, N., Sonnenberg, K., Szabo, E. E., Pacher, P., Csont, T., Schulz, R., Dengler, T. J., Liaudet, L. et al. (2002) Poly(ADP-ribose) polymerase inhibition reduces reperfusion injury after heart transplantation. Circ. Res. **90**, 100–106
41 Pacher, P., Liaudet, L., Bai, P., Virag, L., Mabley, J. G., Hasko, G. and Szabo, C. (2002) Activation of poly(ADP-ribose) polymerase contributes to development of doxorubicin-induced heart failure. J. Pharmacol. Exp. Ther. **300**, 862–867
42 Yates, S. P. and Merrill, A. R. (2001) A catalytic loop within Pseudomonas aeruginosa exotoxin A modulates its transferase activity. J. Biol. Chem. **276**, 35029–35036